Conceptual Design and Analysis of In-Vessel Components for the Materials Plasma Exposure eXperiment (MPEX)

Arnold Lumsdaine, Claire Luttrell, Dean McGinnis, Kirby Logan, Robby Hicks, Steve Meitner, and Juergen Rapp

***Abstract*— The materials plasma exposure experiment (MPEX) is a linear plasma divertor simulator currently undergoing conceptual design. The facility will expose material samples to steady-state plasma fluxes to examine plasma–material interactions (PMIs) that are expected in the next generation of fusion devices. The plasmas will be generated by a helicon source, with electron and ion heating sources of up to 800 kW possible. The peak heat fluxes of the target are expected to be up to 10 MW/m^2. The facility will be capable of handling low-activation neutron-irradiated samples in order to examine the multivariate effects of neutron damage and plasma fluence. Neutron-irradiated samples are planned to be roughly of 10-mm diameter; however, plasma-facing components up to 60 × 600 mm can be accommodated. The steady-state nature of the device will require the magnetic confinement of the plasma to be achieved with superconducting magnets, with a maximum on-axis field of 2.5 T. In addition, since MPEX will be a steady-state device, in-vessel components need to be water cooled. The primary in-vessel components will be the target, the dump plate, the limiter, the skimmers, and the microwave absorber. The conceptual design of these components is presented here, including analyses that confirm that the designs are adequate to meet the requirements of MPEX operation.**

***Index Terms*— High heat flux, in-vessel components, linear plasma facilities, materials testing, plasma–materials interaction (PMI).**

I. Introduction

THE divertor region of next-step fusion facilities will experience an extreme environment that will include high ion fluences, high heat fluxes, and neutron irradiation [1]. The lack of test facilities that are capable of simulating this integrated environment limits the development of fusion components and understanding the plasma–material interactions (PMIs). The need for these next-step facilities that can test these multivariate effects has been identified as a necessary step in the path to fusion energy [2], [3]. Linear plasma facilities have been used for a variety of PMI studies [4], [5]. A new linear facility, the materials plasma exposure experiment (MPEX), has undergone conceptual design at the Oak Ridge National Laboratory [6]–[8], and is expected to be able to apply fusion-relevant plasma fluxes and fluences to *a priori* neutron-irradiated samples. Neutron irradiation will be performed at the high flux isotope reactor (HFIR), which will limit the irradiation of sample articles to roughly 10-mm diameter [9]. Larger components, up to 60 × 600 mm, could be tested as well.

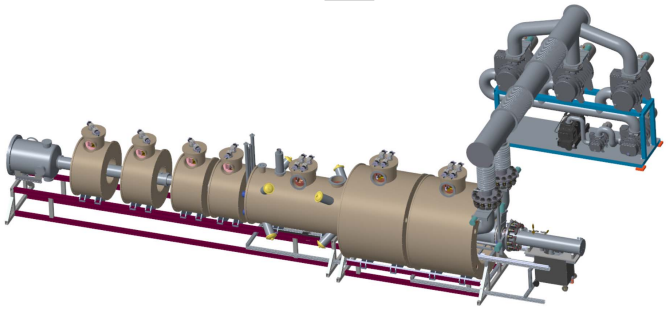

Fig. 1. Conceptual design of MPEX.

A CAD model of the conceptual design of MPEX is shown in Fig. 1. Seven cryostats hold 21 superconducting coils, which will allow for steady-state operation, up to 10^6 s, in order to reach high ion fluxes. The magnetic fields on axis are up to 2.5 T for the electron cyclotron and ion cyclotron heating systems [10]. The plasma is created with a 200-kW helicon source with 400-kW, 70-GHz electron cyclotron heating and 400-kW ion cyclotron heating. Gas species can be hydrogen, deuterium, helium, neon, or a gaseous mixture.

Various in-vessel components are required for MPEX, as shown in Fig. 2. The plasma terminates on a **target**, which sits in a PMI chamber. The target is where the primary PMI samples will be located. The target will receive steady-state heat fluxes of up to 10 MW/m^2 over a 10-cm plasma diameter, and are so much actively cooled. The magnetic field at the target will be 1 T. Because the target will include a 10-mm irradiated coupon, it must be capable of being assembled in a glove box and handled remotely. The peak surface temperature of the sample coupon will be between 800 °C and 1500 °C. The analysis of the target has been presented previously [11], so it is not included here. The **dump plate** will catch the other end of the bi-direction helicon plasma, so it is located at the

Manuscript received June 27, 2019; revised October 25, 2019; accepted November 26, 2019. This manuscript has been authored in part by UT-Battelle, LLC, under contract DE-AC05-00OR22725 with the US Department of Energy (DOE). The US government retains and the publisher, by accepting the article for publication, acknowledges that the US government retains a nonexclusive, paid-up, irrevocable, worldwide license to publish or reproduce the published form of this manuscript, or allow others to do so, for US government purposes. DOE will provide public access to these results of federally sponsored research in accordance with the DOE Public Access Plan (http://energy.gov/downloads/doe-public-access-plan). The review of this article was arranged by Senior Editor G. H. Neilson. *(Corresponding author: Arnold Lumsdaine.)*

The authors are with the Oak Ridge National Laboratory, Oak Ridge, TN 37831 USA (e-mail: lumsdainea@ornl.gov).

Color versions of one or more of the figures in this article are available online at http://ieeexplore.ieee.org.

Digital Object Identifier 10.1109/TPS.2019.2958269

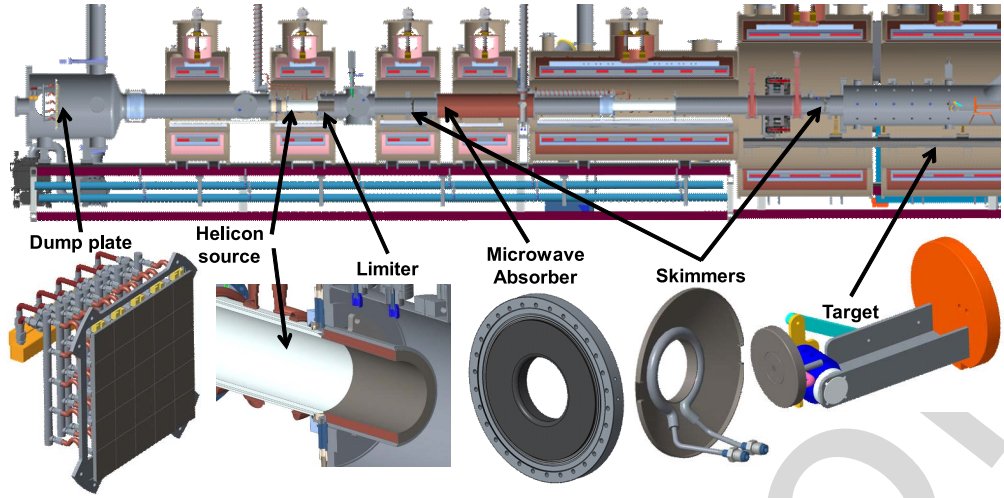

Fig. 2. Cross section of MPEX, with water-cooled in-vessel components shown.

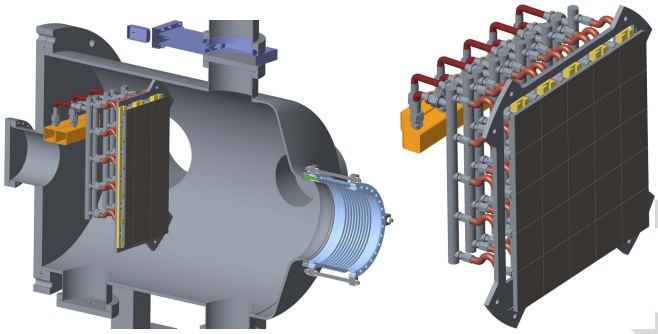

(a) (b)

Fig. 3. (a) Cross section of the dump plate within the dump tank. (b) Dump plate, made of 25 tiles.

opposite end of the device from the target. It should exhaust heat without releasing impurities into the plasma. The **limiter** will shape the plasma coming from the helicon source toward the target and relieve the sensitive helicon window [12], [13] from some of the heat. The **skimmers** will prevent neutral transport in the vacuum chambers in order to control the neutral pressure in different regions of MPEX [14]. The skimmers control the particle flow, but are not highly heat flux components. The **microwave absorber** will catch stray power from the electron-heating system. The in-vessel components control the power exhaust and the particle flow in the vacuum chamber. All in-vessel components require active cooling. The component descriptions, heat load specifications, and analysis (using ANSYS commercial finite element software) to support the ability of the design to meet the specifications are presented in the sequel.

II. Dump Plate

A. Component Description

The dump plate is a large component, designed to be 50.8 cm by 50.8 cm. A cross section of the placement of the dump plate within the dump tank is shown in Fig. 3(a) and the full dump plate is shown in Fig. 3(b). The dump plate will be constructed from 25 tiles, consisting of three different designs. The center tile is exposed to the highest heat load. To keep the temperatures and stresses at acceptable levels, the center tile is cut such that the surrounding tiles will overlap

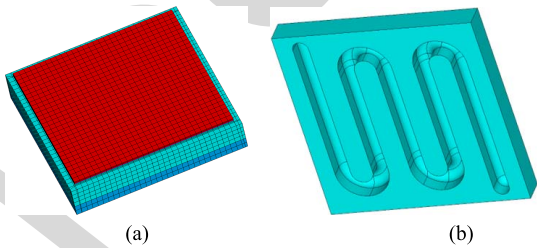

(a) (b)

Fig. 4. Dump plate tile (a) with four material layers and (b) cooling channel milled out of CuCrZr.

the edges of the center. This keeps the heated region of the center tile near the cooling channels. A total of Sixteen of the tiles are cut such that two sides overlap and eight tiles are cut such that one side overlaps. The bottom section of the tiles is 10.2 cm by 10.2 cm. The cutouts and the overhangs are 3.18 mm. The tiles are arranged such that a gap of 0.127 mm exists between the tiles to allow for thermal expansion.

The dump plate tile is made of four layers of different materials and explosively bonded together. The four layers are a 1.5-mm layer of titanium–zirconium–molybdenum (TZM), a 0.5-mm layer of titanium alloy, a 12.7-mm layer of copper–chromium–zirconium (CuCrZr), and a 6.35-mm layer of 304 stainless steel. The titanium layer is necessary between TZM and CuCrZr to allow for the difference in thermal expansion between the two materials. The plate will be cut into 10.2-cm square tiles. The cooling channels will be milled out through the stainless steel and into CuCrZr (shown in Fig. 4), and then a stainless cap will be welded on to create a robust water to vacuum seal. An example of this procedure used for cooling is an ITER electron cyclotron heating component [15]. The cooling channel width is 8 mm across with a radius at the top of the channel. The depth of the channel from the bottom to the top of the radius is 10.2 mm.

B. Heat Load Specification

It is assumed that the power to the dump plate will be equal to the power to the target, which is required to be 31 kW (which is calculated from the project specifications that require a 10-MW/m^2 peak heat flux with a 10-cm diameter plasma). This is likely a conservative assumption as some of

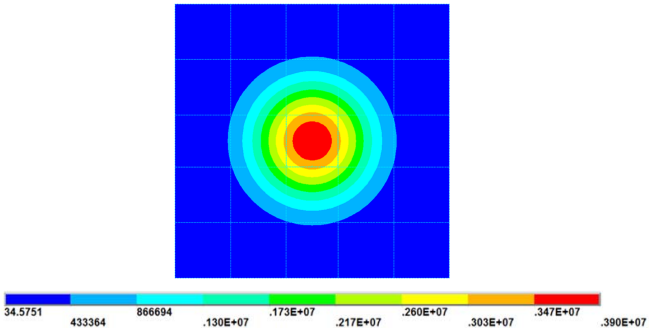

Fig. 5. Heat flux distribution on the dump plate.

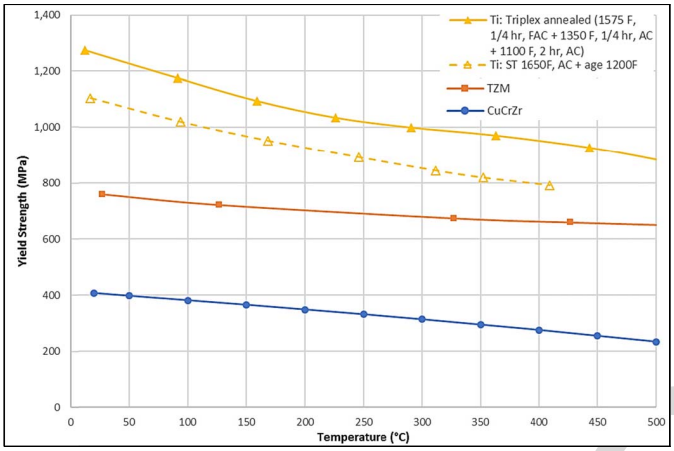

Fig. 6. Yield strength versus temperature for dump plate materials.

the heating systems are expected to heat preferentially toward the target. Furthermore, it is assumed that a much higher parallel heat flux of 40 MW/m^2 at the target is achieved in a 10-cm diameter plasma at the target for studies involving a tilted target. (In reality, these higher parallel heat fluxes are specified to occur in a much smaller 3.5-cm diameter). This would produce a total power of 120 kW. If the dump plate is located at a position in the dump tank such that the plasma diameter is 31.6 cm (which will occur where the field is 10% of the field required for a 10-cm diameter) and the heat is distributed in a Gaussian profile, then the peak heat flux on the plate will be 3.9 MW/m^2. These extremely conservative assumptions will ensure a good safety margin for the design.

C. Component Analysis

The heat load on the dump plate is a Gaussian distribution, with a peak heat flux of 3.9 MW/m^2 and a plasma diameter (10% of peak) of 31.6 cm. The heat flux distribution on the dump plate is shown in Fig. 5. The center tile receives the highest heat load. The tiles adjacent to the center tile receive a high heat load on one edge and a significant gradient. The tiles are cooled with water flowing through cooling channels in each tile. It is assumed that the water velocity in the channels is 6 m/s, which produces a convection coefficient of 24.7 kW/m^{2}K (using the Gnielinski correlation [16]). The assumptions used for the convection coefficient calculation are a water temperature of 25 °C at 0.1-MPa pressure. The hydraulic diameter is calculated to be 9.12 mm.

Material properties as a function of temperature are used in the finite element analysis of the dump plate (with the exception of Poisson's ratio). The yield strength of materials used in the model are shown in Fig. 6. The figure shows the yield strength of TZM, Ti R56260, and CuCrZr versus temperature. The strength of the Ti alloy is shown at two different heat treatments to show a range of values. The yield strength of 304 stainless steel is for quarter hard temper.

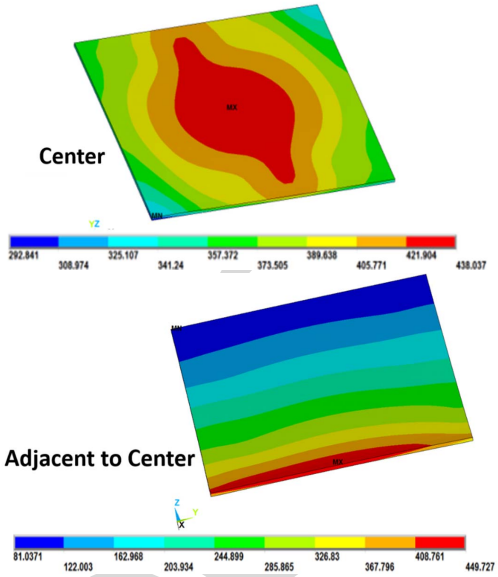

Fig. 7. Temperature contours for the center tile and the adjacent tile.

TABLE I
CENTER TILE ANALYSIS RESULTS

	Temp. (°C)	Von Mises Stress (MPa)	Yield Strength (MPa)
TZM	438	335	658
Ti Alloy	386	265	800
CuCrZr	229	277	338
304 SST	179	349	515

Of the 25 tiles that make up the dump plate, the center tile will receive the highest thermal load. The tiles directly adjacent to the center tile will also receive a high heat load on one side. These two tiles were modeled individually, with the appropriate heat flux applied. The center tile has the highest heat load and the adjacent tiles have a high heat load on the edge.

The top TZM layer has the highest temperature. The temperature profiles in the TZM layer for the center tile and the adjacent tile are shown in Fig. 7. The maximum temperature in the TZM layer is 450 °C. The results show that the peak temperature does not occur in the center tile. It is in the edge of the adjacent tile that extends over the center tile. This region of tile is further away from the cooling channel in the tile, which causes an increased temperature. The maximum temperature in the Ti alloy layer is 413 °C. The maximum temperature in the CuCrZr layer is 277 °C and the maximum temperature in the stainless layer is 186 °C. A summary of peak temperatures is shown in Tables I and II.

Structural analyses are also performed. The structural model used the same mesh as for the thermal analyses. As was done with the thermal analyses, the center tile and the adjacent tile were analyzed. The temperature profiles from the thermal analyses were applied to the structural models. The stresses in

TABLE II
ADJACENT TILE ANALYSIS RESULTS

	Temp. (°C)	Von Mises Stress (MPa)	Yield Strength (MPa)
TZM	450	374	655
Ti Alloy	413	304	790
CuCrZr	277	286	321
304 SST	186	244	515

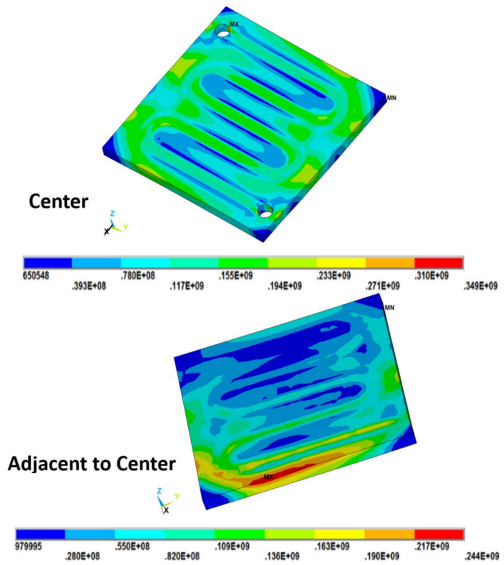

Fig. 8. Stress contours for the center tile and the adjacent tile.

each material level were evaluated and compared to the yield stress for the layer material. The von Mises stresses in the TZM layer for the center tile and the adjacent tile are shown in Fig. 8. The maximum von Mises stress in the TZM layer is 374 MPa. The results show that the peak von Mises stress does not occur in the center tile. It is in the corner of the adjacent tile that extends over the center tile and is farthest away from the cooling channel. The maximum von Mises stress in the Ti alloy layer is 304 MPa. The maximum von Mises stress in the CuCrZr layer is 286 MPa and the maximum von Mises stress in the stainless layer is 349 MPa.

A summary of the peak von Mises stress in each material layer is shown in Tables I and II. The tables also show the yield strength of the material at the peak temperature in the material layer of the tile. The properties vary depending on the heat treatment. Although the peak stress is close to the yield stress in a few cases, it is worth noting that the heat load applied is a factor of four higher than what is expected.

III. LIMITER

A. Component Description

The limiter shapes the plasma coming from the source, which will interact convectively with the plasma and can be used to reduce the heat flux on the helicon antenna window. The positioning of the limiter with the helicon assembly is shown in Fig. 9. Since the limiter will experience high heat fluxes, it will have a CuCrZr core that will be water cooled. The plasma interacting surface will be tungsten (1-mm thickness) with a thin interlayer between tungsten and CuCrZr in order to mitigate the thermal expansion mismatch. The outside shell will be stainless steel. The limiter will be manufactured

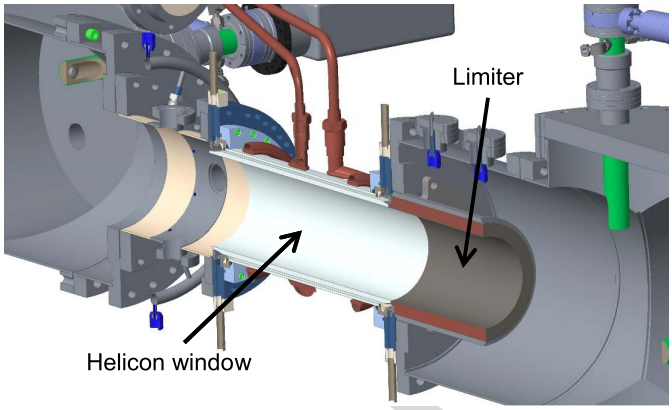

Fig. 9. Conceptual design CAD model of the helicon antenna and the limiter.

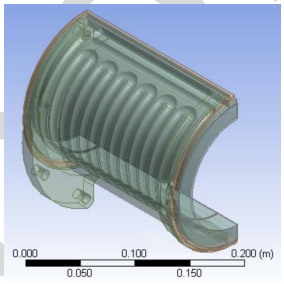

Fig. 10. Conceptual design CAD model of the limiter, with a transparent outer steel jacket to make cooling passages visible.

by first explosively bonding a stainless steel and a CuCrZr plate. This will then be rolled to the appropriate curvature (11.4-cm diameter). The steel will be machined out down to CuCrZr, and then cooling channels machined into CuCrZr. A stainless-steel cover will be welded onto the remaining stainless steel in order to enclose the water cooling passages. The cooling water inlet and outlet will be then in the stainless cover. The inner side of CuCrZr will be machined in order to develop the secondary curvature along the length of the limiter. Then, a plasma spray process will be used on the inside of CuCrZr to deposit a thin interlayer (0.25 mm) and then a layer of tungsten (1 mm). This process will make one-half of the limiter (see Fig. 10). An identical piece can be fit to this to make the full limiter.

B. Heat Load Specification

Based on the experimental results on Proto-MPEX [17], it is anticipated that 40% of the applied power to the helicon antenna will be deposited on the window and the limiter. If it is assumed that this power is evenly divided between these two components, then each will be loaded with 40 kW.

C. Component Analysis

If the limiter is to take 40 kW of heat, it will average 1.08 MW/m^2 on the inner face. A finite element model was created, assuming this heat flux and a 5-m/s water velocity (0.178-kg/s mass flow rate) yields a 21.1-kW/m^{2}K convection coefficient on the cooling passages of the limiter (calculated from the Gnielinski correlation). The thermal results are shown in Fig. 11. A peak temperature of 192 °C is well within the material limits. In the future work, computational fluid dynamics (CFD) simulations will be performed in order to obtain

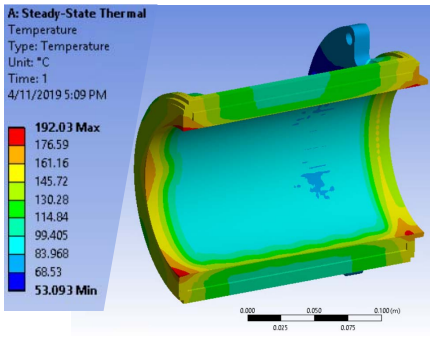

Fig. 11. Temperature contours for limiter analysis.

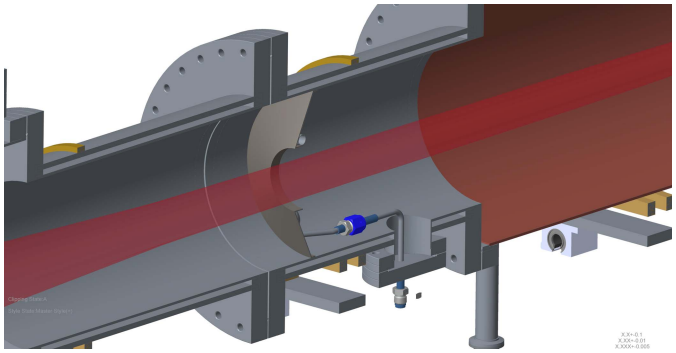

Fig. 12. One skimmer shown upstream of the electron-heating region (indicated in brown), with the plasma shown.

more accurate thermal results, the water temperature, and the hydraulic characteristics. Stress analysis will be performed to confirm the structural robustness. In addition, a prototype will be built and tested in a high heat-flux test facility.

IV. Skimmer

A. Component Description

The skimmers are intended to prevent the transport of neutrals through the device, so that the required low-pressure region can be achieved for electron and ion heating. The effectiveness of skimmers has been demonstrated in Proto-MPEX [18]. Skimmers will be placed on either side of the plasma heating region. The skimmers will be plasma facing, but are not intended to interact with the plasma, and should experience virtually no convective load. Thus, the expected heat flux is less than that of the limiter (see Fig. 12). The skimmers will be made of CuCrZr.

B. Heat Load Specification

In Proto-MPEX, the skimmer was estimated to receive a load of 0.22 kW for a 101.3-kW power to the helicon antenna [17]. A 1.33-kW total heat load on the skimmer is applied in order to account for the additional helicon power in MPEX (factor of 2) and the power from other heating sources (conservatively, a factor of 3). This heat is applied primarily to the inner face (plasma facing region) of the skimmer, with a 100-kW/m^2 heat flux, with another 35 kW/m^2 applied to the "flange" face of the skimmer.

C. Component Analysis

The cooling tubes have a 6.35-mm inner diameter with a thickness of 0.5 mm. It is assumed that the water velocity

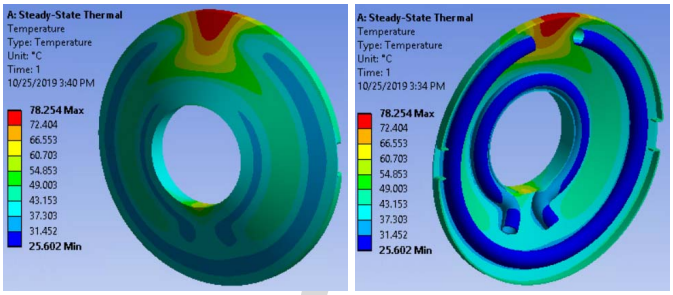

Fig. 13. Temperature contours for the skimmer.

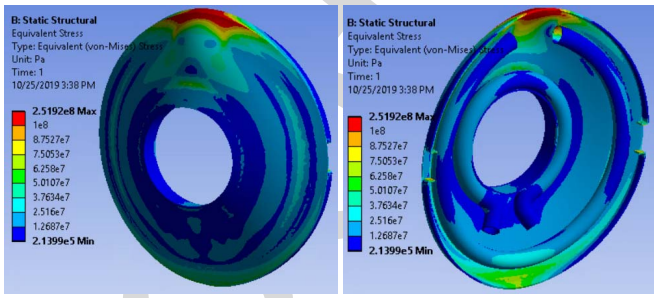

Fig. 14. Stress contours for the skimmer.

in the tube is 2 m/s, which produces a convection coefficient of 8.7 kW/m^{2}K (using the Gnielinski correlation). The thermal results are shown in Fig. 13, with a peak temperature of 78 °C. The stress results are shown in Fig. 14. The peak stress is 252 MPa, but this is in a very local region (which might result in local yielding). The stress is under 100 MPa over almost all of the components.

V. Microwave Absorber

A. Component Description

Up to 400 kW of 70-GHz microwave power is expected to be launched into a copper or copper-coated vessel. The absorption of copper for this frequency microwave is less than 0.1%, so the portion of this power that is not absorbed into the plasma is expected to reflect around the vessel. In order to minimize the amount of reflected power that reaches other (stainless steel) portions of the vacuum vessel which have higher absorption, a microwave absorber is planned, which will be located on both the dump and target sides of the copper-plated, stainless-steel chamber. The microwave absorber will require high heat flux-handing capability and low electrical conductivity.

The conceptual design of the microwave absorber is shown in Fig. 15. The flange of the absorber is stainless steel, with a CuCrZr heat sink brazed to it. A cooling channel can be milled into the heat sink, and a stainless-steel cover plate welded to the stainless flange. A microwave-absorbing material, such as TiO_2, will be plasma sprayed onto the other side of the heat sink, which faces the microwave source.

B. Heat Load Specification

For specifying the heat loads, a worst case assumption is made here that none of the power is absorbed in the plasma. Assuming a scenario of all 400 kW absorbed equally on the target or dump-side graphite microwave absorber would imply an average heat flux of ~3.6 MW/m^2.

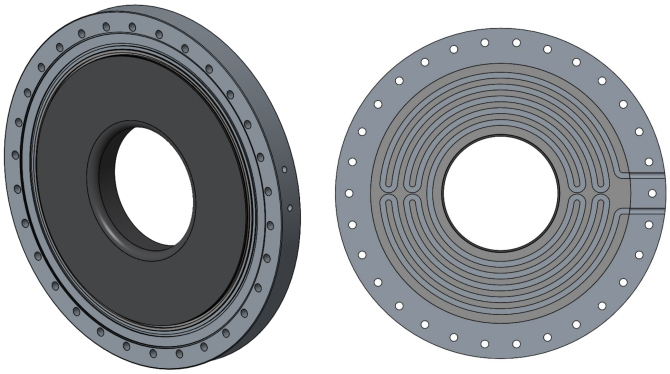

(a) (b)

Fig. 15. Microwave absorber showing the (a) absorbing side and (b) cooling channel.

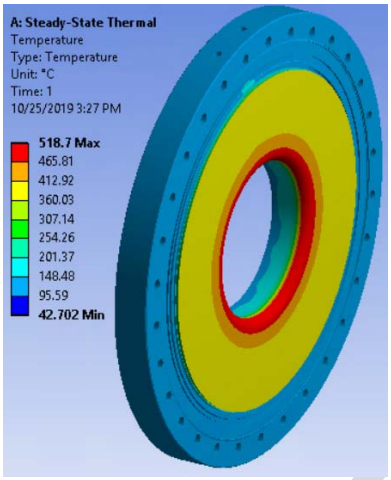

Fig. 16. Temperature contours of the microwave absorber.

C. Component Analysis

The cooling channel milled into the heat sink has a straight side that is 12.7 mm deep and 6.35 mm wide, ending in an additional 6.35-mm diameter semicircle. The pattern is shown in Fig. 14(b). The hydraulic diameter for the cross section is 4.35 mm. For a water velocity of 5 m/s, the mass flow rate would be 0.481 kg/s. The convection coefficient (calculated using the Gneilinski correlation assuming room temperature water) would be 22 kW/m^2-K. A thermal analysis result is shown in Fig. 16, with a peak temperature on the absorbing face of 519 °C. The peak temperature in the CuCrZr heat sink is 323 °C. In the future work, CFD simulations will be performed in order to obtain more accurate thermal results, water temperature, and hydraulic characteristics. Stress analysis will be performed to confirm the structural robustness.

VI. Conclusion and Next Steps

The conceptual design for the in-vessel components of the MPEX linear plasma facility has been completed. Analyses have been performed to demonstrate the essential feasibility of these components to meet their design requirements. The following steps are planned in the next design phase.

1) CFD of the dump plate tile, limiter, and microwave absorber.
2) Structural analysis of the limiter and the microwave absorber (including transient loading/unloading).
3) Examination of a broader set of loading cases for the limiter (to confirm robustness for varying heat fluxes).
4) Testing of the limiter concept in a steady-state linear plasma facility.
5) Manufacturing prototype dump plate tile, limiter, and microwave absorber, and test under prototypical heat fluxes, including thermal cycling.

References

[1] J. Rapp, "The challenges of plasma material interactions in nuclear fusion devices and potential solutions," *Fusion Sci. Technol.*, vol. 72, no. 3, pp. 211–221, 2017.

[2] (2013). *Report of the FESAC Subcommittee on the Priorities of the Magnetic Fusion Energy Science Program*. [Online]. Available: http://science.energy.gov/~/media/fes/fesac/pdf/2013/Final-Report-02102013.pdf

[3] J. Rapp *et al.*, "The development of the plasma-material interaction facilities for the future of fusion technology," *Fusion Sci. Technol.*, vol. 64, no. 2, pp. 237–244, 2013.

[4] R. P. Doerner, G. R. Tynan, and K. Schmid, "Implications of PMI and wall material choice on fusion reactor tritium self-sufficiency," *Nucl. Mater. Energy*, vol. 18, pp. 56–61, 2019, doi: 10.1016/j.nme.2018.12.006.

[5] M. Shimada, C. N. Taylor, R. J. Pawelko, L. C. Cadwallader, and B. J. Merrill, "Tritium plasma experiment upgrade and improvement of surface diagnostic capabilities at star facility for enhancing tritium and nuclear PMI sciences," *Fusion Sci. Technol.*, vol. 71, no. 3, pp. 310–315, 2017.

[6] J. Rapp *et al.*, "The development of the material plasma exposure experiment," *IEEE Trans. Plasma Sci.*, vol. 44, no. 12, pp. 3456–3464, Dec. 2016.

[7] J. Rapp *et al.*, "Latest results from proto-MPEX and the future plans for MPEX," *Fusion Sci. Technol.*, vol. 75, no. 7, pp. 654–663, 2019.

[8] J. Rapp *et al.*, "Developing the science and technology for the material plasma exposure experiment," *Nucl. Fusion*, vol. 57, no. 11, 2017, Art. no. 116001.

[9] R. J. Ellis and J. Rapp, "Neutron-irradiated samples as test materials for MPEX," *Fusion Sci. Technol.*, vol. 68, no. 4, pp. 750–757, 2015.

[10] R. Duckworth *et al.*, "Progress in magnet design activities for the material plasma exposure experiment," *Fusion Eng. Des.*, vol. 124, pp. 211–214, Nov. 2017.

[11] A. Lumsdaine, J. B. Tipton, D. L. Youchison, V. Varma, K. Logan, and J. Rapp, "High heat-flux target design for the materials plasma exposure experiment," *Fusion Sci. Technol.*, vol. 75, no. 7, pp. 674–682, 2019.

[12] A. Lumsdaine *et al.*, "Design and analysis of an actively cooled window for a high-power helicon plasma source," *IEEE Trans. Plasma Sci.*, vol. 47, no. 1, pp. 902–909, Jan. 2019.

[13] M. Showers, T. M. Biewer, J. Caughman, D. C. Donovan, R. H. Goulding, and J. Rapp, "Heat flux estimates of power balance on Proto-MPEX with IR imaging," *Rev. Sci. Instrum.*, vol. 87, no. 11, pp. 1–4, Nov. 2016, Art. no. 11D412, doi: 10.1063/1.4959953.

[14] A. Lumsdaine *et al.*, "Vacuum system and modeling for the materials plasma exposure experiment," *Fusion Sci. Technol.*, vol. 72, no. 4, pp. 581–587, 2017.

[15] D. Youchison, A. Melin, A. Lumsdaine, C. Schaich, and G. Hanson, "ITER ECH waveguide switch design and analysis," *Fusion Sci. Technol.*, vol. 72, no. 3, pp. 324–330, 2017.

[16] F. P. Incropera and D. P. DeWitt, *Fundamentals of Heat and Mass Transfer*, 5th ed. Hoboken, NJ, USA: Wiley, 2002, p. 492.

[17] M. Showers *et al.*, "Power accounting of plasma discharges in the linear device Proto-MPEX," *Plasma Phys. Control. Fusion*, vol. 60, no. 6, p. 10, 2018, Art. no. 065001, doi: 10.1088/1361-6587/aab7c8.

[18] J. F. Caneses *et al.*, "Differential pumping requirements for the light-ion helicon source and heating systems of Proto-MPEX," *Phys. Plasma*, vol. 25, pp. 1–11, no. 8, 2018, Art. no. 083518, doi: 10.1063/1.5001519.

Conceptual Design and Analysis of In-Vessel Components for the Materials Plasma Exposure eXperiment (MPEX)

Arnold Lumsdaine, Claire Luttrell, Dean McGinnis, Kirby Logan, Robby Hicks, Steve Meitner, and Juergen Rapp

***Abstract*— The materials plasma exposure experiment (MPEX) is a linear plasma divertor simulator currently undergoing conceptual design. The facility will expose material samples to steady-state plasma fluxes to examine plasma–material interactions (PMIs) that are expected in the next generation of fusion devices. The plasmas will be generated by a helicon source, with electron and ion heating sources of up to 800 kW possible. The peak heat fluxes of the target are expected to be up to 10 MW/m^2. The facility will be capable of handling low-activation neutron-irradiated samples in order to examine the multivariate effects of neutron damage and plasma fluence. Neutron-irradiated samples are planned to be roughly of 10-mm diameter; however, plasma-facing components up to 60 × 600 mm can be accommodated. The steady-state nature of the device will require the magnetic confinement of the plasma to be achieved with superconducting magnets, with a maximum on-axis field of 2.5 T. In addition, since MPEX will be a steady-state device, in-vessel components need to be water cooled. The primary in-vessel components will be the target, the dump plate, the limiter, the skimmers, and the microwave absorber. The conceptual design of these components is presented here, including analyses that confirm that the designs are adequate to meet the requirements of MPEX operation.**

***Index Terms*— High heat flux, in-vessel components, linear plasma facilities, materials testing, plasma–materials interaction (PMI).**

I. Introduction

THE divertor region of next-step fusion facilities will experience an extreme environment that will include high ion fluences, high heat fluxes, and neutron irradiation [1]. The lack of test facilities that are capable of simulating this integrated environment limits the development of fusion components and understanding the plasma–material interactions (PMIs). The need for these next-step facilities that can test these multivariate effects has been identified as a necessary step in the path to fusion energy [2], [3]. Linear plasma facilities have been used for a variety of PMI studies [4], [5]. A new linear facility, the materials plasma exposure experiment (MPEX), has undergone conceptual design at the Oak Ridge National Laboratory [6]–[8], and is expected to be able to apply fusion-relevant plasma fluxes and fluences to *a priori* neutron-irradiated samples. Neutron irradiation will be performed at the high flux isotope reactor (HFIR), which will limit the irradiation of sample articles to roughly 10-mm diameter [9]. Larger components, up to 60 × 600 mm, could be tested as well.

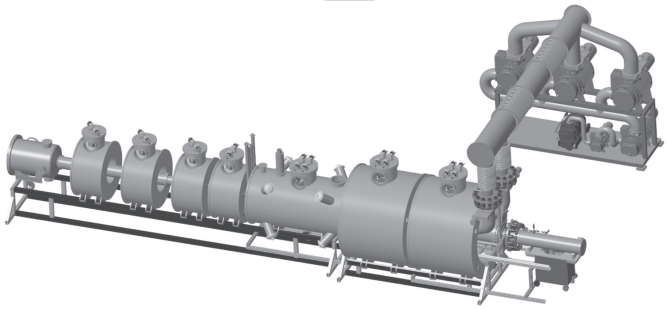

Fig. 1. Conceptual design of MPEX.

A CAD model of the conceptual design of MPEX is shown in Fig. 1. Seven cryostats hold 21 superconducting coils, which will allow for steady-state operation, up to 10^6 s, in order to reach high ion fluxes. The magnetic fields on axis are up to 2.5 T for the electron cyclotron and ion cyclotron heating systems [10]. The plasma is created with a 200-kW helicon source with 400-kW, 70-GHz electron cyclotron heating and 400-kW ion cyclotron heating. Gas species can be hydrogen, deuterium, helium, neon, or a gaseous mixture.

Various in-vessel components are required for MPEX, as shown in Fig. 2. The plasma terminates on a **target**, which sits in a PMI chamber. The target is where the primary PMI samples will be located. The target will receive steady-state heat fluxes of up to 10 MW/m^2 over a 10-cm plasma diameter, and are so much actively cooled. The magnetic field at the target will be 1 T. Because the target will include a 10-mm irradiated coupon, it must be capable of being assembled in a glove box and handled remotely. The peak surface temperature of the sample coupon will be between 800 °C and 1500 °C. The analysis of the target has been presented previously [11], so it is not included here. The **dump plate** will catch the other end of the bi-direction helicon plasma, so it is located at the

Manuscript received June 27, 2019; revised October 25, 2019; accepted November 26, 2019. This manuscript has been authored in part by UT-Battelle, LLC, under contract DE-AC05-00OR22725 with the US Department of Energy (DOE). The US government retains and the publisher, by accepting the article for publication, acknowledges that the US government retains a nonexclusive, paid-up, irrevocable, worldwide license to publish or reproduce the published form of this manuscript, or allow others to do so, for US government purposes. DOE will provide public access to these results of federally sponsored research in accordance with the DOE Public Access Plan (http://energy.gov/downloads/doe-public-access-plan). The review of this article was arranged by Senior Editor G. H. Neilson. *(Corresponding author: Arnold Lumsdaine.)*

The authors are with the Oak Ridge National Laboratory, Oak Ridge, TN 37831 USA (e-mail: lumsdainea@ornl.gov).

Color versions of one or more of the figures in this article are available online at http://ieeexplore.ieee.org.

Digital Object Identifier 10.1109/TPS.2019.2958269

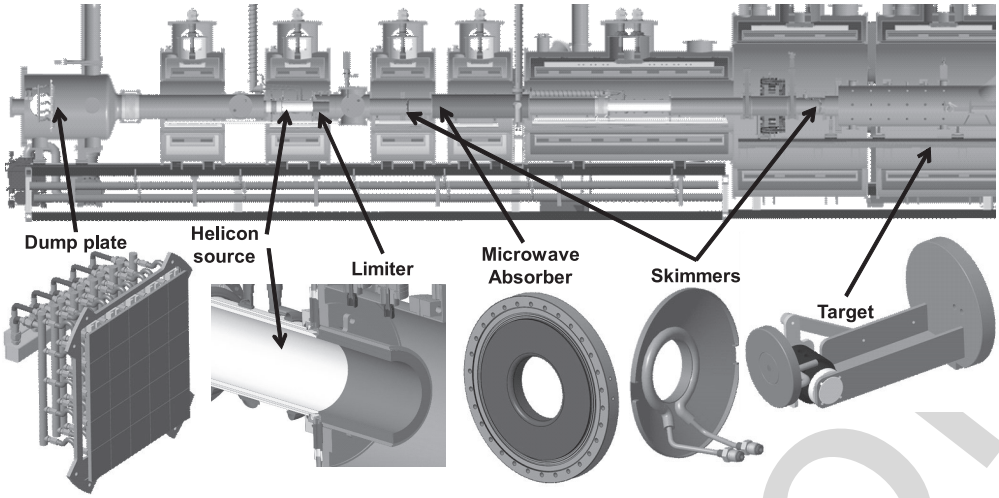

Fig. 2. Cross section of MPEX, with water-cooled in-vessel components shown.

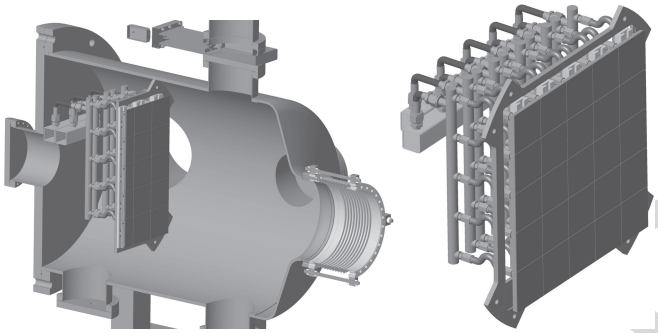

(a) (b)

Fig. 3. (a) Cross section of the dump plate within the dump tank. (b) Dump plate, made of 25 tiles.

opposite end of the device from the target. It should exhaust heat without releasing impurities into the plasma. The **limiter** will shape the plasma coming from the helicon source toward the target and relieve the sensitive helicon window [12], [13] from some of the heat. The **skimmers** will prevent neutral transport in the vacuum chambers in order to control the neutral pressure in different regions of MPEX [14]. The skimmers control the particle flow, but are not highly heat flux components. The **microwave absorber** will catch stray power from the electron-heating system. The in-vessel components control the power exhaust and the particle flow in the vacuum chamber. All in-vessel components require active cooling. The component descriptions, heat load specifications, and analysis (using ANSYS commercial finite element software) to support the ability of the design to meet the specifications are presented in the sequel.

II. Dump Plate

A. Component Description

The dump plate is a large component, designed to be 50.8 cm by 50.8 cm. A cross section of the placement of the dump plate within the dump tank is shown in Fig. 3(a) and the full dump plate is shown in Fig. 3(b). The dump plate will be constructed from 25 tiles, consisting of three different designs. The center tile is exposed to the highest heat load. To keep the temperatures and stresses at acceptable levels, the center tile is cut such that the surrounding tiles will overlap

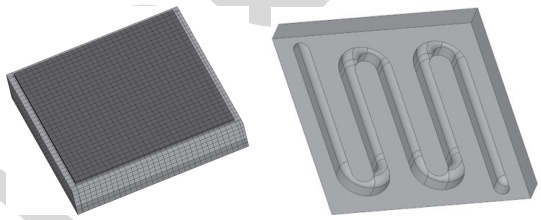

(a) (b)

Fig. 4. Dump plate tile (a) with four material layers and (b) cooling channel milled out of CuCrZr.

the edges of the center. This keeps the heated region of the center tile near the cooling channels. A total of Sixteen of the tiles are cut such that two sides overlap and eight tiles are cut such that one side overlaps. The bottom section of the tiles is 10.2 cm by 10.2 cm. The cutouts and the overhangs are 3.18 mm. The tiles are arranged such that a gap of 0.127 mm exists between the tiles to allow for thermal expansion.

The dump plate tile is made of four layers of different materials and explosively bonded together. The four layers are a 1.5-mm layer of titanium–zirconium–molybdenum (TZM), a 0.5-mm layer of titanium alloy, a 12.7-mm layer of copper–chromium–zirconium (CuCrZr), and a 6.35-mm layer of 304 stainless steel. The titanium layer is necessary between TZM and CuCrZr to allow for the difference in thermal expansion between the two materials. The plate will be cut into 10.2-cm square tiles. The cooling channels will be milled out through the stainless steel and into CuCrZr (shown in Fig. 4), and then a stainless cap will be welded on to create a robust water to vacuum seal. An example of this procedure used for cooling is an ITER electron cyclotron heating component [15]. The cooling channel width is 8 mm across with a radius at the top of the channel. The depth of the channel from the bottom to the top of the radius is 10.2 mm.

B. Heat Load Specification

It is assumed that the power to the dump plate will be equal to the power to the target, which is required to be 31 kW (which is calculated from the project specifications that require a 10-MW/m^2 peak heat flux with a 10-cm diameter plasma). This is likely a conservative assumption as some of

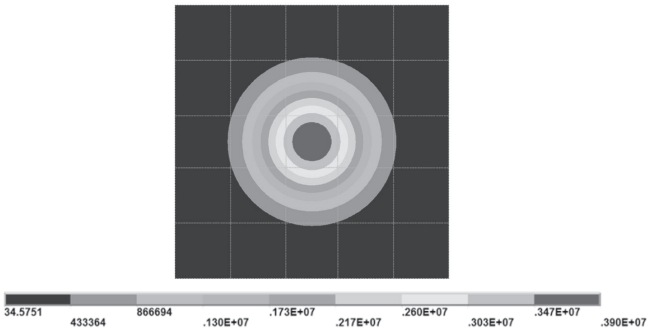

Fig. 5. Heat flux distribution on the dump plate.

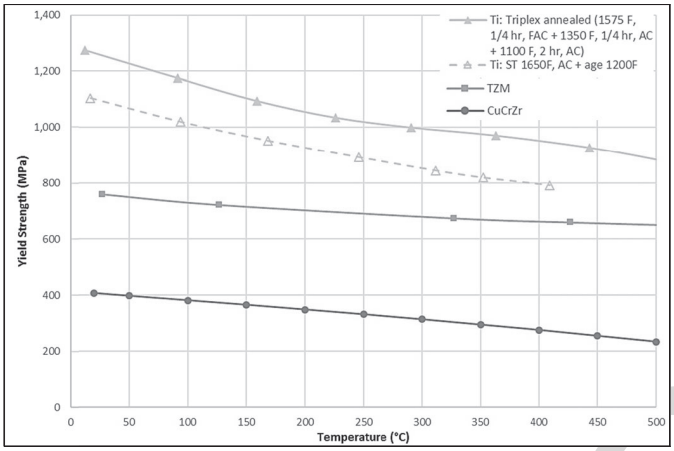

Fig. 6. Yield strength versus temperature for dump plate materials.

the heating systems are expected to heat preferentially toward the target. Furthermore, it is assumed that a much higher parallel heat flux of 40 MW/m^2 at the target is achieved in a 10-cm diameter plasma at the target for studies involving a tilted target. (In reality, these higher parallel heat fluxes are specified to occur in a much smaller 3.5-cm diameter). This would produce a total power of 120 kW. If the dump plate is located at a position in the dump tank such that the plasma diameter is 31.6 cm (which will occur where the field is 10% of the field required for a 10-cm diameter) and the heat is distributed in a Gaussian profile, then the peak heat flux on the plate will be 3.9 MW/m^2. These extremely conservative assumptions will ensure a good safety margin for the design.

C. Component Analysis

The heat load on the dump plate is a Gaussian distribution, with a peak heat flux of 3.9 MW/m^2 and a plasma diameter (10% of peak) of 31.6 cm. The heat flux distribution on the dump plate is shown in Fig. 5. The center tile receives the highest heat load. The tiles adjacent to the center tile receive a high heat load on one edge and a significant gradient. The tiles are cooled with water flowing through cooling channels in each tile. It is assumed that the water velocity in the channels is 6 m/s, which produces a convection coefficient of 24.7 kW/m^{2}K (using the Gnielinski correlation [16]). The assumptions used for the convection coefficient calculation are a water temperature of 25 °C at 0.1-MPa pressure. The hydraulic diameter is calculated to be 9.12 mm.

Material properties as a function of temperature are used in the finite element analysis of the dump plate (with the exception of Poisson's ratio). The yield strength of materials used in the model are shown in Fig. 6. The figure shows the yield strength of TZM, Ti R56260, and CuCrZr versus temperature. The strength of the Ti alloy is shown at two different heat treatments to show a range of values. The yield strength of 304 stainless steel is for quarter hard temper.

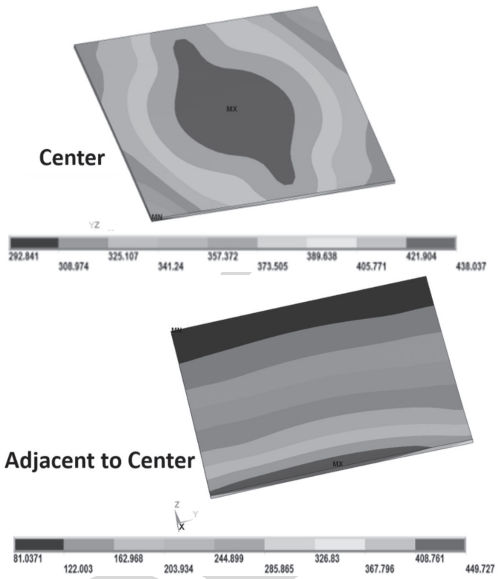

Fig. 7. Temperature contours for the center tile and the adjacent tile.

TABLE I
CENTER TILE ANALYSIS RESULTS

	Temp. (°C)	Von Mises Stress (MPa)	Yield Strength (MPa)
TZM	438	335	658
Ti Alloy	386	265	800
CuCrZr	229	277	338
304 SST	179	349	515

Of the 25 tiles that make up the dump plate, the center tile will receive the highest thermal load. The tiles directly adjacent to the center tile will also receive a high heat load on one side. These two tiles were modeled individually, with the appropriate heat flux applied. The center tile has the highest heat load and the adjacent tiles have a high heat load on the edge.

The top TZM layer has the highest temperature. The temperature profiles in the TZM layer for the center tile and the adjacent tile are shown in Fig. 7. The maximum temperature in the TZM layer is 450 °C. The results show that the peak temperature does not occur in the center tile. It is in the edge of the adjacent tile that extends over the center tile. This region of tile is further away from the cooling channel in the tile, which causes an increased temperature. The maximum temperature in the Ti alloy layer is 413 °C. The maximum temperature in the CuCrZr layer is 277 °C and the maximum temperature in the stainless layer is 186 °C. A summary of peak temperatures is shown in Tables I and II.

Structural analyses are also performed. The structural model used the same mesh as for the thermal analyses. As was done with the thermal analyses, the center tile and the adjacent tile were analyzed. The temperature profiles from the thermal analyses were applied to the structural models. The stresses in

TABLE II
ADJACENT TILE ANALYSIS RESULTS

	Temp. (°C)	Von Mises Stress (MPa)	Yield Strength (MPa)
TZM	450	374	655
Ti Alloy	413	304	790
CuCrZr	277	286	321
304 SST	186	244	515

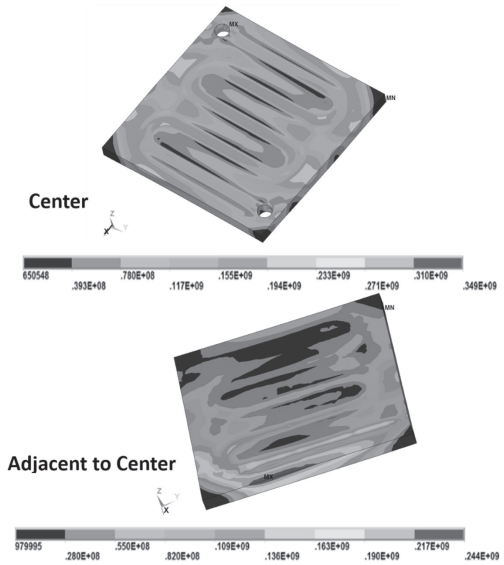

Fig. 8. Stress contours for the center tile and the adjacent tile.

each material level were evaluated and compared to the yield stress for the layer material. The von Mises stresses in the TZM layer for the center tile and the adjacent tile are shown in Fig. 8. The maximum von Mises stress in the TZM layer is 374 MPa. The results show that the peak von Mises stress does not occur in the center tile. It is in the corner of the adjacent tile that extends over the center tile and is farthest away from the cooling channel. The maximum von Mises stress in the Ti alloy layer is 304 MPa. The maximum von Mises stress in the CuCrZr layer is 286 MPa and the maximum von Mises stress in the stainless layer is 349 MPa.

A summary of the peak von Mises stress in each material layer is shown in Tables I and II. The tables also show the yield strength of the material at the peak temperature in the material layer of the tile. The properties vary depending on the heat treatment. Although the peak stress is close to the yield stress in a few cases, it is worth noting that the heat load applied is a factor of four higher than what is expected.

III. LIMITER

A. Component Description

The limiter shapes the plasma coming from the source, which will interact convectively with the plasma and can be used to reduce the heat flux on the helicon antenna window. The positioning of the limiter with the helicon assembly is shown in Fig. 9. Since the limiter will experience high heat fluxes, it will have a CuCrZr core that will be water cooled. The plasma interacting surface will be tungsten (1-mm thickness) with a thin interlayer between tungsten and CuCrZr in order to mitigate the thermal expansion mismatch. The outside shell will be stainless steel. The limiter will be manufactured

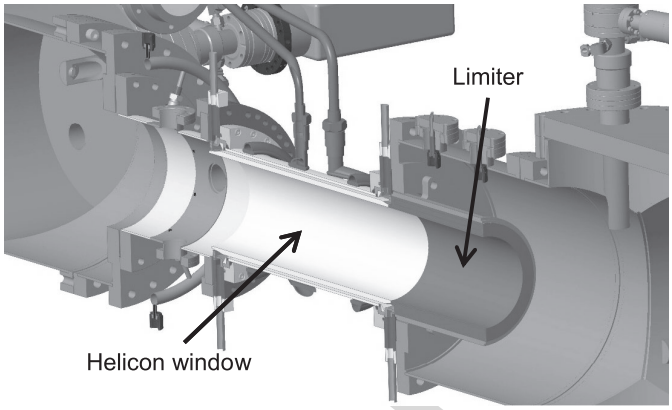

Fig. 9. Conceptual design CAD model of the helicon antenna and the limiter.

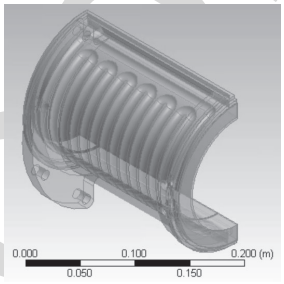

Fig. 10. Conceptual design CAD model of the limiter, with a transparent outer steel jacket to make cooling passages visible.

by first explosively bonding a stainless steel and a CuCrZr plate. This will then be rolled to the appropriate curvature (11.4-cm diameter). The steel will be machined out down to CuCrZr, and then cooling channels machined into CuCrZr. A stainless-steel cover will be welded onto the remaining stainless steel in order to enclose the water cooling passages. The cooling water inlet and outlet will be then in the stainless cover. The inner side of CuCrZr will be machined in order to develop the secondary curvature along the length of the limiter. Then, a plasma spray process will be used on the inside of CuCrZr to deposit a thin interlayer (0.25 mm) and then a layer of tungsten (1 mm). This process will make one-half of the limiter (see Fig. 10). An identical piece can be fit to this to make the full limiter.

B. Heat Load Specification

Based on the experimental results on Proto-MPEX [17], it is anticipated that 40% of the applied power to the helicon antenna will be deposited on the window and the limiter. If it is assumed that this power is evenly divided between these two components, then each will be loaded with 40 kW.

C. Component Analysis

If the limiter is to take 40 kW of heat, it will average 1.08 MW/m^2 on the inner face. A finite element model was created, assuming this heat flux and a 5-m/s water velocity (0.178-kg/s mass flow rate) yields a 21.1-kW/m^{2}K convection coefficient on the cooling passages of the limiter (calculated from the Gnielinski correlation). The thermal results are shown in Fig. 11. A peak temperature of 192 °C is well within the material limits. In the future work, computational fluid dynamics (CFD) simulations will be performed in order to obtain

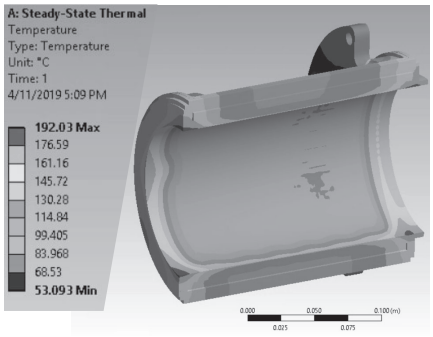

Fig. 11. Temperature contours for limiter analysis.

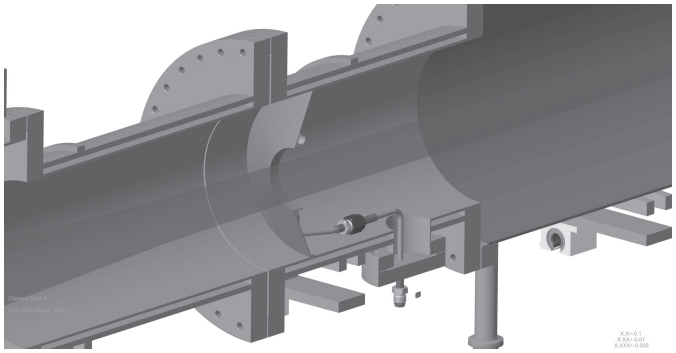

Fig. 12. One skimmer shown upstream of the electron-heating region (indicated in brown), with the plasma shown.

more accurate thermal results, the water temperature, and the hydraulic characteristics. Stress analysis will be performed to confirm the structural robustness. In addition, a prototype will be built and tested in a high heat-flux test facility.

IV. Skimmer

A. Component Description

The skimmers are intended to prevent the transport of neutrals through the device, so that the required low-pressure region can be achieved for electron and ion heating. The effectiveness of skimmers has been demonstrated in Proto-MPEX [18]. Skimmers will be placed on either side of the plasma heating region. The skimmers will be plasma facing, but are not intended to interact with the plasma, and should experience virtually no convective load. Thus, the expected heat flux is less than that of the limiter (see Fig. 12). The skimmers will be made of CuCrZr.

B. Heat Load Specification

In Proto-MPEX, the skimmer was estimated to receive a load of 0.22 kW for a 101.3-kW power to the helicon antenna [17]. A 1.33-kW total heat load on the skimmer is applied in order to account for the additional helicon power in MPEX (factor of 2) and the power from other heating sources (conservatively, a factor of 3). This heat is applied primarily to the inner face (plasma facing region) of the skimmer, with a 100-kW/m^2 heat flux, with another 35 kW/m^2 applied to the "flange" face of the skimmer.

C. Component Analysis

The cooling tubes have a 6.35-mm inner diameter with a thickness of 0.5 mm. It is assumed that the water velocity in the tube is 2 m/s, which produces a convection coefficient of 8.7 kW/m^{2}K (using the Gnielinski correlation). The thermal results are shown in Fig. 13, with a peak temperature of 78 °C. The stress results are shown in Fig. 14. The peak stress is 252 MPa, but this is in a very local region (which might result in local yielding). The stress is under 100 MPa over almost all of the components.

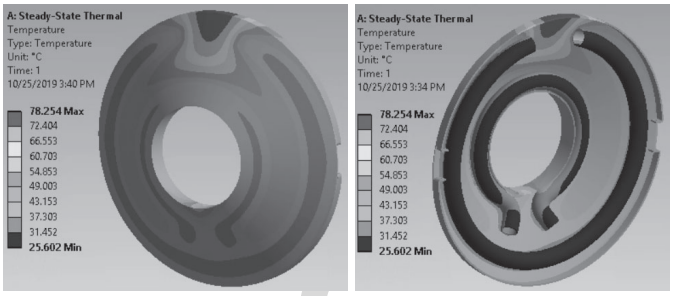

Fig. 13. Temperature contours for the skimmer.

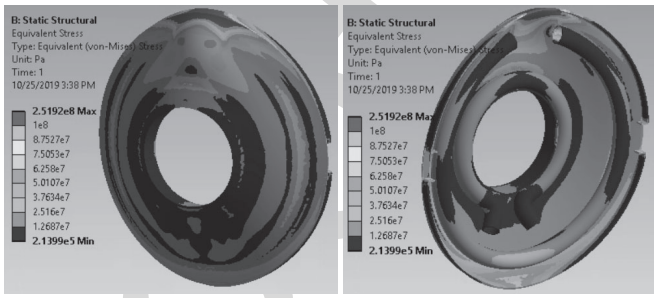

Fig. 14. Stress contours for the skimmer.

V. Microwave Absorber

A. Component Description

Up to 400 kW of 70-GHz microwave power is expected to be launched into a copper or copper-coated vessel. The absorption of copper for this frequency microwave is less than 0.1%, so the portion of this power that is not absorbed into the plasma is expected to reflect around the vessel. In order to minimize the amount of reflected power that reaches other (stainless steel) portions of the vacuum vessel which have higher absorption, a microwave absorber is planned, which will be located on both the dump and target sides of the copper-plated, stainless-steel chamber. The microwave absorber will require high heat flux-handing capability and low electrical conductivity.

The conceptual design of the microwave absorber is shown in Fig. 15. The flange of the absorber is stainless steel, with a CuCrZr heat sink brazed to it. A cooling channel can be milled into the heat sink, and a stainless-steel cover plate welded to the stainless flange. A microwave-absorbing material, such as TiO_2, will be plasma sprayed onto the other side of the heat sink, which faces the microwave source.

B. Heat Load Specification

For specifying the heat loads, a worst case assumption is made here that none of the power is absorbed in the plasma. Assuming a scenario of all 400 kW absorbed equally on the target or dump-side graphite microwave absorber would imply an average heat flux of ∼3.6 MW/m^2.

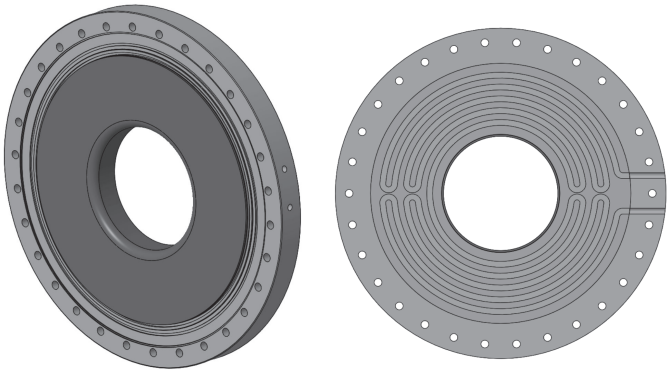

(a) (b)

Fig. 15. Microwave absorber showing the (a) absorbing side and (b) cooling channel.

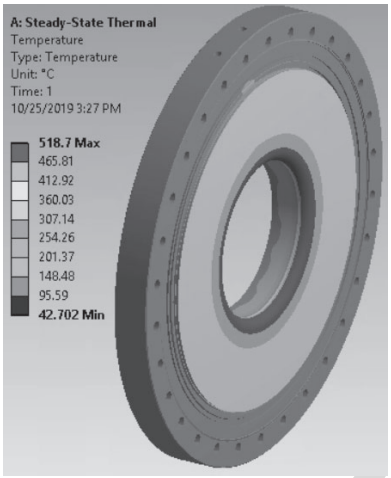

Fig. 16. Temperature contours of the microwave absorber.

C. Component Analysis

The cooling channel milled into the heat sink has a straight side that is 12.7 mm deep and 6.35 mm wide, ending in an additional 6.35-mm diameter semicircle. The pattern is shown in Fig. 14(b). The hydraulic diameter for the cross section is 4.35 mm. For a water velocity of 5 m/s, the mass flow rate would be 0.481 kg/s. The convection coefficient (calculated using the Gneilinski correlation assuming room temperature water) would be 22 kW/m^2-K. A thermal analysis result is shown in Fig. 16, with a peak temperature on the absorbing face of 519 °C. The peak temperature in the CuCrZr heat sink is 323 °C. In the future work, CFD simulations will be performed in order to obtain more accurate thermal results, water temperature, and hydraulic characteristics. Stress analysis will be performed to confirm the structural robustness.

VI. Conclusion and Next Steps

The conceptual design for the in-vessel components of the MPEX linear plasma facility has been completed. Analyses have been performed to demonstrate the essential feasibility of these components to meet their design requirements. The following steps are planned in the next design phase.

1) CFD of the dump plate tile, limiter, and microwave absorber.
2) Structural analysis of the limiter and the microwave absorber (including transient loading/unloading).
3) Examination of a broader set of loading cases for the limiter (to confirm robustness for varying heat fluxes).
4) Testing of the limiter concept in a steady-state linear plasma facility.
5) Manufacturing prototype dump plate tile, limiter, and microwave absorber, and test under prototypical heat fluxes, including thermal cycling.

References

[1] J. Rapp, "The challenges of plasma material interactions in nuclear fusion devices and potential solutions," *Fusion Sci. Technol.*, vol. 72, no. 3, pp. 211–221, 2017.

[2] (2013). *Report of the FESAC Subcommittee on the Priorities of the Magnetic Fusion Energy Science Program*. [Online]. Available: http://science.energy.gov/~/media/fes/fesac/pdf/2013/Final-Report-02102013.pdf

[3] J. Rapp *et al.*, "The development of the plasma-material interaction facilities for the future of fusion technology," *Fusion Sci. Technol.*, vol. 64, no. 2, pp. 237–244, 2013.

[4] R. P. Doerner, G. R. Tynan, and K. Schmid, "Implications of PMI and wall material choice on fusion reactor tritium self-sufficiency," *Nucl. Mater. Energy*, vol. 18, pp. 56–61, 2019, doi: 10.1016/j.nme.2018.12.006.

[5] M. Shimada, C. N. Taylor, R. J. Pawelko, L. C. Cadwallader, and B. J. Merrill, "Tritium plasma experiment upgrade and improvement of surface diagnostic capabilities at star facility for enhancing tritium and nuclear PMI sciences," *Fusion Sci. Technol.*, vol. 71, no. 3, pp. 310–315, 2017.

[6] J. Rapp *et al.*, "The development of the material plasma exposure experiment," *IEEE Trans. Plasma Sci.*, vol. 44, no. 12, pp. 3456–3464, Dec. 2016.

[7] J. Rapp *et al.*, "Latest results from proto-MPEX and the future plans for MPEX," *Fusion Sci. Technol.*, vol. 75, no. 7, pp. 654–663, 2019.

[8] J. Rapp *et al.*, "Developing the science and technology for the material plasma exposure experiment," *Nucl. Fusion*, vol. 57, no. 11, 2017, Art. no. 116001.

[9] R. J. Ellis and J. Rapp, "Neutron-irradiated samples as test materials for MPEX," *Fusion Sci. Technol.*, vol. 68, no. 4, pp. 750–757, 2015.

[10] R. Duckworth *et al.*, "Progress in magnet design activities for the material plasma exposure experiment," *Fusion Eng. Des.*, vol. 124, pp. 211–214, Nov. 2017.

[11] A. Lumsdaine, J. B. Tipton, D. L. Youchison, V. Varma, K. Logan, and J. Rapp, "High heat-flux target design for the materials plasma exposure experiment," *Fusion Sci. Technol.*, vol. 75, no. 7, pp. 674–682, 2019.

[12] A. Lumsdaine *et al.*, "Design and analysis of an actively cooled window for a high-power helicon plasma source," *IEEE Trans. Plasma Sci.*, vol. 47, no. 1, pp. 902–909, Jan. 2019.

[13] M. Showers, T. M. Biewer, J. Caughman, D. C. Donovan, R. H. Goulding, and J. Rapp, "Heat flux estimates of power balance on Proto-MPEX with IR imaging," *Rev. Sci. Instrum.*, vol. 87, no. 11, pp. 1–4, Nov. 2016, Art. no. 11D412, doi: 10.1063/1.4959953.

[14] A. Lumsdaine *et al.*, "Vacuum system and modeling for the materials plasma exposure experiment," *Fusion Sci. Technol.*, vol. 72, no. 4, pp. 581–587, 2017.

[15] D. Youchison, A. Melin, A. Lumsdaine, C. Schaich, and G. Hanson, "ITER ECH waveguide switch design and analysis," *Fusion Sci. Technol.*, vol. 72, no. 3, pp. 324–330, 2017.

[16] F. P. Incropera and D. P. DeWitt, *Fundamentals of Heat and Mass Transfer*, 5th ed. Hoboken, NJ, USA: Wiley, 2002, p. 492.

[17] M. Showers *et al.*, "Power accounting of plasma discharges in the linear device Proto-MPEX," *Plasma Phys. Control. Fusion*, vol. 60, no. 6, p. 10, 2018, Art. no. 065001, doi: 10.1088/1361-6587/aab7c8.

[18] J. F. Caneses *et al.*, "Differential pumping requirements for the light-ion helicon source and heating systems of Proto-MPEX," *Phys. Plasma*, vol. 25, pp. 1–11, no. 8, 2018, Art. no. 083518, doi: 10.1063/1.5001519.